

# Light-Induced Thickening of Photoreceptor Outer Segment Layer Detected by Ultra-High Resolution OCT Imaging

Yichao Li,<sup>1</sup> Robert N. Fariss,<sup>2</sup> Jennifer W. Qian,<sup>3</sup> Ethan D. Cohen,<sup>4</sup> and Haohua Qian<sup>1</sup>

<sup>1</sup>Visual Function Core, National Eye Institute, National Institutes of Health, Bethesda, Maryland, United States

<sup>2</sup>Biological Imaging Core, National Eye Institute, National Institutes of Health, Bethesda, Maryland, United States

<sup>3</sup>College of Arts & Sciences, University of Virginia, Charlottesville, Virginia, United States

<sup>4</sup>Division of Biomedical Physics, Office of Science and Engineering Labs, Center for Devices and Radiological Health, Food and Drug Administration, Silver Spring, Maryland, United States

Correspondence: Haohua Qian, Visual Function Core, National Eye Institute, National Institutes of Health, Bethesda, MD 20892, USA; haohua.qian@nih.gov.

Submitted: October 29, 2015

Accepted: February 6, 2016

Citation: Li Y, Fariss RN, Qian JW, Cohen ED, Qian H. Light-induced thickening of photoreceptor outer segment layer detected by ultra-high resolution OCT imaging. *Invest Ophthalmol Vis Sci.* 2016;57:OCT105–OCT111. DOI:10.1167/iovs.15-18539

**PURPOSE.** We examined if light induces changes in the retinal structure that can be observed using optical coherence tomography (OCT).

**METHODS.** Normal C57BL/6J mice (age 3–6 months) adapted to either room light (15 minutes to ~5 hours, 50–500 lux) or darkness (overnight) were imaged using a Biotigen UHR-OCT system. Confocal histologic images were obtained from mice killed under light- or dark-adapted conditions.

**RESULTS.** The OCT image of eyes adapted to room light exhibited significant increases ( $6.1 \pm 0.8 \mu\text{m}$ ,  $n = 13$ ) in total retina thickness compared to the same eyes after overnight dark adaptation. These light-adapted retinal thickness changes occurred mainly in the outer retina, with the development of a hyporeflective band between the RPE and photoreceptor-tip layers. Histologic analysis revealed a light-evoked elongation between the outer limiting membrane and Bruch's membrane from  $45.8 \pm 1.7 \mu\text{m}$  in the dark ( $n = 5$ ) to  $52.1 \pm 3.7 \mu\text{m}$  ( $n = 5$ ) in the light. Light-adapted retinas showed an increase of actin staining in RPE apical microvilli at the same location as the hyporeflective band observed in OCT images. Elongation of the outer retina could be detected even with brief light exposures, increasing  $2.1 \pm 0.3 \mu\text{m}$  after 15 minutes ( $n = 9$ ), and  $4.1 \pm 1.0 \mu\text{m}$  after 2 hours ( $n = 6$ ). Conversely, dark-adaptation caused outer retinal shortening of  $1.4 \pm 0.4 \mu\text{m}$  ( $n = 7$ ) and  $3.0 \pm 0.5 \mu\text{m}$  ( $n = 8$ ) after 15 minutes and 2 hours, respectively.

**CONCLUSIONS.** Light-adaptation induces an increase in the thickness of the outer retina and the appearance of a hyporeflective band in the OCT image. This is consistent with previous reports of light-induced fluid accumulation in the subretinal space.

**Keywords:** optical coherence tomography, subretinal space, light/dark adaptation, outer segments, retinal pigment epithelium

Optical coherence tomography (OCT) has been used widely as a noninvasive tool to provide optical sections of biological tissues, and has become a standard tool in the diagnosis and monitoring of retinal disease progression in the clinic and laboratory.<sup>1–5</sup> Optical coherence tomography imaging uses a broadband infrared light to analyze the reflectance properties of a tissue sample.<sup>6</sup> Recent advances in OCT imaging technologies, especially with the application of spectral-domain OCT, have provided higher resolution images with better contrast of the retinal structure. It now is possible to resolve multiple (typically 4) hyperreflective bands in the human outer retina.<sup>7–9</sup> Starting from the inner retina, these bands are termed the outer limiting membrane (OLM), inner segment (IS)/outer segment (OS) junction or IS/ellipsoid (IS/ep),<sup>7,10</sup> photoreceptor tips (PRT) in interaction with the RPE (retinal pigment epithelium) processes, and RPE cell and Bruch's membrane (BM) complex.<sup>8</sup>

Optical coherence tomography images have provided valuable insights into the pathophysiology of many eye diseases, particular those involving photoreceptor and/or RPE impairment. Recent studies have linked the integrity of the OCT bands in the

outer retina with normal visual function.<sup>9,11</sup> However, it is unclear whether any of these bands is influenced by light conditions. Determining how OCT bands change with light-adaptation (LA) could improve our understanding of the origin of OCT signals and interpretation of variations in clinical OCT images, which could help in the interpretation of retinal diseases.

The investigation of OCT images under different light conditions remains largely unexplored. Most OCT image studies are performed in the LA condition under normal room light. We compared OCT images of the mouse retina under LA and dark-adaptation (DA) conditions, and correlated them with retinal histology. Our results suggested a novel application for OCT imaging as a noninvasive tool for studying dynamic morphologic changes at the photoreceptor-RPE interface.

## METHODS

### Animal

All procedures involving animals were conducted under an approved National Institutes of Health (NIH; Bethesda, MD,

USA) animal care protocol and in accordance with the ARVO Statement for the Use of Animals in Ophthalmic and Vision Research. Adult wild type mice (C57B/6J), 3 to 6 months old, of either sex were used in this study. The mice were kept in regular animal housing under a 50 lux 14:10 hour light/dark cycle.

### OCT Imaging

An ultrahigh resolution 850 nm (bandwidth 160 nm) OCT system with an axial resolution of 1.6  $\mu\text{m}$  in tissue (Envisu UHR2200; Bioptigen, Durham, NC, USA) operating in EDI mode was used to obtain optical sections of the retina. Mice were anesthetized with ketamine (100 mg/kg) and xylazine (6 mg/kg). Eye position was adjusted to place the optic nerve head in the center of the OCT scan. For imaging LA animals, all procedures were done under normal procedure room illumination (500 lux). For long-term (~5 hours) LA, mice were placed in regular animal housing (50 lux), and kept in the procedure room (500 lux) for short-term (15 minutes and 2 hours) LA. For DA animals, all procedures were performed under dim red light. Optical coherence tomography images were analyzed using ImageJ (NIH) and Diver 2.4 software (Bioptigen). Data are presented as mean  $\pm$  SD.

### Histology and Immunocytochemistry

Light-adapted mice were perfused with fixative and enucleated under room illumination while DA mice were fixed similarly under dim red illumination. Under deep anesthesia of ketamine and xylazine, animals were perfused intracardially with a mixed aldehyde fixative (2% formaldehyde + 1% glutaraldehyde in PBS buffer, pH 7.3). Eyes were enucleated and then immersed in additional fixative for 24 hours. Posterior eye cups were embedded in 7% agarose (Sigma-Aldrich Corp., St. Louis, MO, USA) and sectioned at 100  $\mu\text{m}$  using a vibratome.<sup>12</sup> Sections were stained for retinal, RPE, and choroidal landmarks with 4',6-diamidino-2-phenylindole (DAPI; Invitrogen, Carlsbad, CA, USA), Alexa Fluor488 phalloidin (Invitrogen), and Alexa Fluor 555 wheat germ agglutinin (WGA; Invitrogen) by incubating overnight in the probes. Confocal images were collected at a fixed distance from the optic nerve using a Zeiss LSM 780 confocal microscope (Carl Zeiss Microscopy, Thornwood NY, USA). Data are presented as mean  $\pm$  SD.

## RESULTS

### Retinal OCT Image Under LA and DA conditions

Using high-resolution OCT imaging, we examined the optical structure of the mouse retina under LA and DA conditions. Figure 1A shows an example of an averaged B-scan OCT image (40 B-scans of 1000 A-scans, same location) taken through the optic nerve head from the same mouse eye in the LA condition (upper) and after overnight DA (lower). For better comparison of the two conditions, a smaller region marked by blue lines shows images at the same eccentricity compared side-by-side (Fig. 1B). For the inner retina, from the nerve fiber layer (NFL) to the outer limiting membrane (OLM), it is clear that the OCT images obtained under LA and DA conditions are very similar. This similarity also can be observed in the intensity-depth profile shown in Figure 1C which plots averaged values of 10 pixels in the center regions of each OCT image shown in Figure 1B. For the OCT intensity-depth profiles derived from the LA (red trace) and DA (blue trace) images, the troughs and peaks of the inner retina (from NFL to OLM) are largely superimposed.

However, for the outer retina, the OCT images showed significant differences in the LA/DA conditions. Figure 1D illustrates enlarged images of the distal retina for a region outlined by the green dashed line in Figure 1B. Four distinct bands could be identified conclusively on OCT images obtained in either condition, that is OLM, IS/ep, PRT, and RPE. In the LA retina, an additional hyporeflective OCT band separated the PRT and RPE bands (Figs. 1B, 1D, red arrows). However, this hyporeflective band was undetectable in the DA retina, where the PRT and RPE bands abutted each other. Consequently, the insertion of an additional hyporeflective band between the PRT and RPE bands in the LA image appeared to account for the increase in the optical thickness of the "outer retina" (from the OLM to the RPE) in the OCT images when compared to their DA counterparts. On the intensity-depth profiles of the outer retinal region shown in Figure 1E, an additional trough of hyporeflectivity is observed in the curve of the light-adapted image (red arrow). This hyporeflective band appears to displace the RPE and choroid peaks to a more distal location in the LA OCT image (red trace) compared to the DA condition (blue trace).

Figure 2 summarizes quantitative measurements of retinal layer thickness in the OCT images obtained under LA and DA conditions. Two methods were used for measuring the retinal layer thickness. First, the retinal layers were measured manually using the conventions shown in Figure 2A. For each eye, layer thicknesses were measured at a retinal location approximately 0.4 mm away from the optic nerve head for left and right image fields. Values from horizontal and vertical B-scans were averaged. Optical coherence tomography measurements of the thickness of the whole retina and the inner and outer regions under LA and DA conditions are shown in Figure 2B. There is a significant difference in total retinal thickness (measured from NFL to RPE) between the LA and DA OCT images. On average, the overall thickness of the LA retina increased by  $6.1 \pm 0.8 \mu\text{m}$  ( $n = 13$  eyes,  $P < 0.001$ ) over the DA retina. The retinal thickness increase was detected mainly in the outer retina (OLM to RPE;  $6.8 \pm 0.7 \mu\text{m}$ ,  $P < 0.001$ ), with no significant LA/DA thickness changes in the inner retina (NFL to OLM). Adopting the names previously used to define 3 outer retinal sublayers in human OCT images,<sup>7,8</sup> we measured these layers in the mouse for LA/DA thickness changes as illustrated in Figure 2A: the IS, from the OLM to the distal edge of IS/ep band; the outer segment equivalent length (OSEL; described by Abramoff et al.<sup>15</sup>), from the distal edge of the IS/ep to the apical edge of RPE band; and the RPE, thickness of the RPE band. As shown in Figure 2C, no adaptation differences are detected in the thickness of the IS and RPE layers. On the other hand, the OSEL exhibited significant thickening in the LA versus DA condition, with an average difference of  $5.7 \pm 0.6 \mu\text{m}$  ( $n = 13$ ,  $P < 0.001$ ).

The second approach for measuring retinal layer thickness used the Diver auto-segmentation software (Bioptigen), which produces 8 segmented lines with 7 retinal layers (illustrated in Fig. 2D). When the volume scan (C-scan,  $1.4 \times 1.4$  mm, 1000 A-scan/B-scan  $\times$  100 B-scan) OCT images from a subgroup of mice are analyzed by Diver, consistent elongation of the OSEL layer is observed, whereas no significant change in thickness is detected for the other 6 retinal layers (data not shown). Figure 2E shows the averaged LA/DA thickness changes of the OSEL layer from the OCT C-scan at various ETDRS grid (100/300/600  $\mu\text{m}$ ) retinal regions (insert in Fig. 2E). Except for grid 1, which is occupied by the optic nerve head, similar magnitudes of thickness changes are detected for the other 8 retinal regions of the mouse fundus, implying that LA elicits a uniform lengthening of the OSEL thickness across the whole retina. The averaged LA/DA OSEL thickness difference of the 8 grid regions

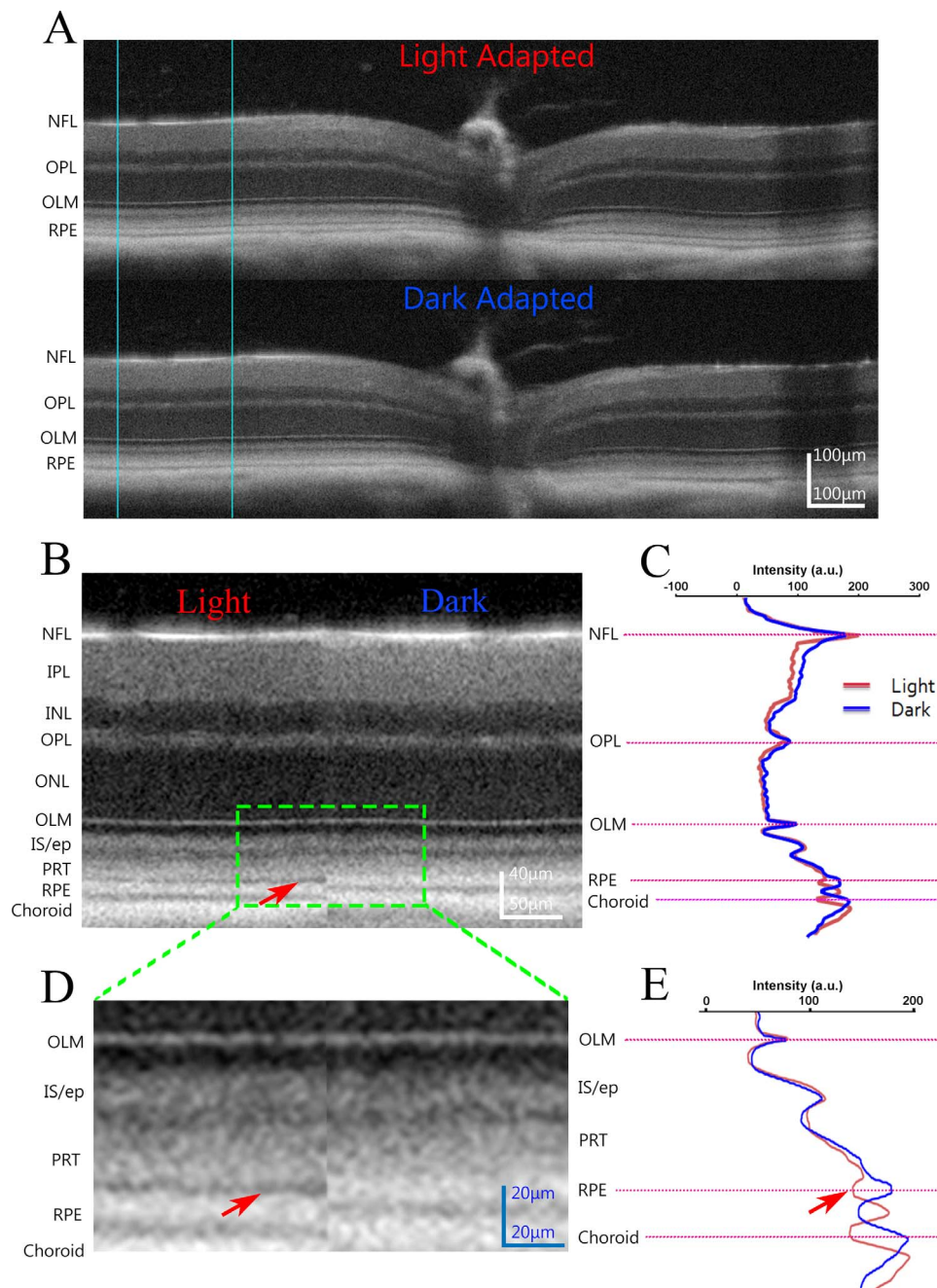


**FIGURE 1.** Example of UHR-OCT retinal images obtained from the same mouse eye under LA and DA conditions. (A) Averaged B-scan of the mouse retina through optic nerve head in the LA (*upper*), and DA (*bottom*) conditions. (B) Side-by-side comparison of the OCT images for the same local retinal region (outlined by *blue lines* in [A]) under LA and DA conditions. *Green box* marks area shown at high magnification in (D). *Red arrow* points to a hyporeflective layer between PRT and RPE layers only present in the OCT image obtained under LA conditions. (C) The intensity-depth profile (derived from averaged values of 10 pixels in the center regions) of images shown in (B) for the LA (*red line*) and DA (*blue line*) conditions. (E) Magnified intensity-depth profile from OLM to choroid. *Red arrow* points to an additional trough only observed in the intensity profile of LA OCT images. IPL, inner plexiform layer; INL, inner nuclear layer; OPL, outer plexiform layer.

was  $5.3 \pm 0.6 \mu\text{m}$  ( $n = 8$ ), a value similar in magnitude to our manual measurements (Fig. 2C).

### Effects of Light or Dark Exposure Duration on OCT Images

We examined the effects of different LA/DA exposure durations on the OSEL length measured in OCT images, and the results are summarized in Figure 2F. To study the effects of LA, mice

were dark-adapted overnight, and baseline images were taken under DA conditions. Then, the animals were exposed to 500 lux room light for either 15 minutes or 2 hours, and OCT images were obtained. To investigate the effect of dark exposure, mice were initially light-adapted  $> 5$  hours. After baseline OCT images were taken under room lights, mice were placed in darkness for either 15 minutes or 2 hours and OCT images obtained in the dark. Within 15 minutes' exposure to either LA or DA, small but significant OSEL length changes

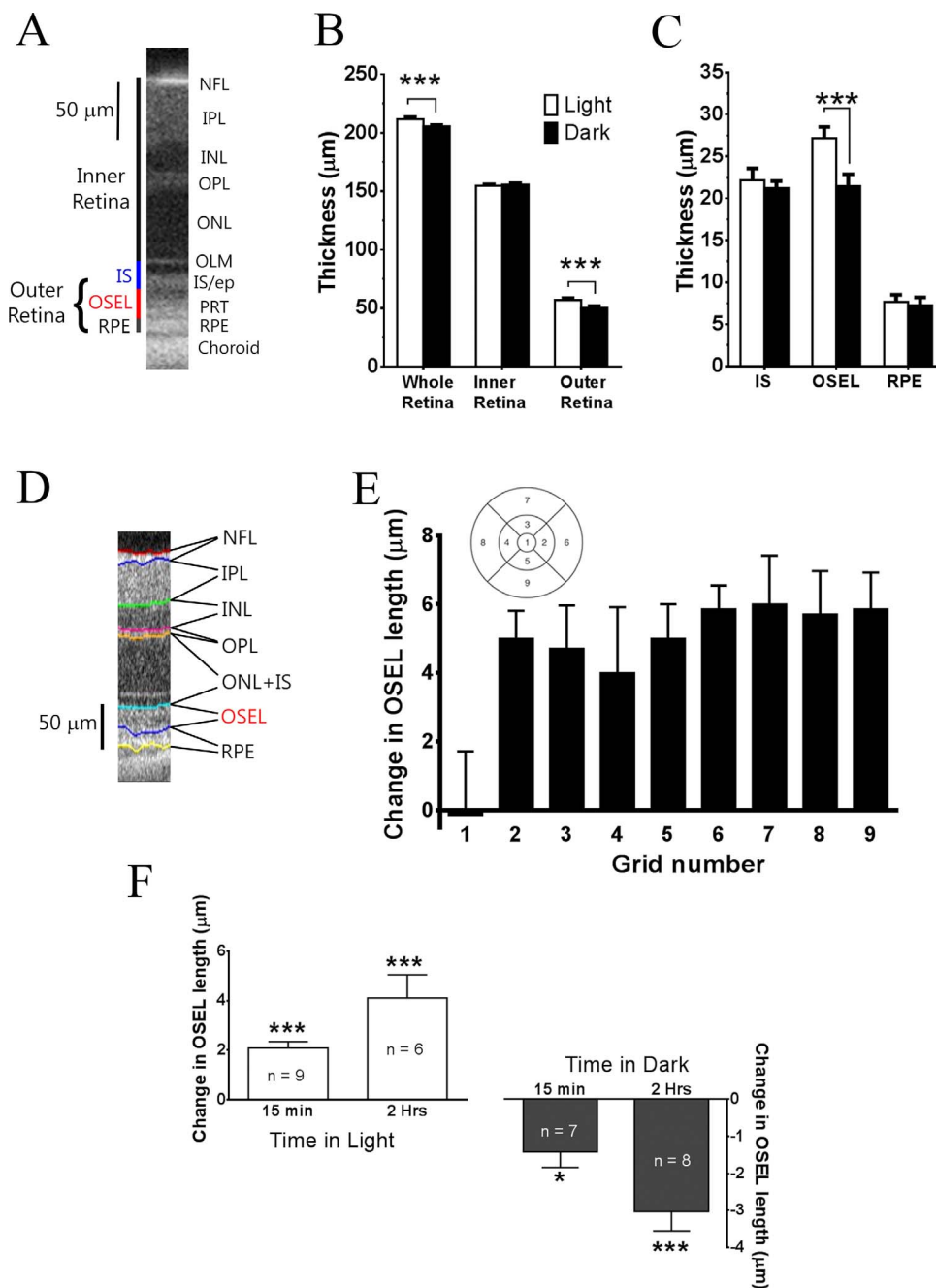


**FIGURE 2.** Light induces increases in the thickness of the retinal layers when measured using UHR-OCT compared to the DA condition. (A) Schematic diagram illustrate positions used for measure length for each retinal regions from OCT B-scan images. (B) Bar graph of averaged thickness for total retina, and inner and outer retinal regions under LA and DA conditions ( $n = 13$ ). (C) Averaged outer retinal layer thickness under LA and DA conditions. The LA thickness increases were observed largely in the OSEL. (D) Schematic diagram illustrates the auto-segmented lines and retinal regions measured with the Bioprogen Diver analysis software. (E) Differences in OSEL length between LA and DA conditions measured using Diver software from volume scan OCT images ( $n = 8$ ) aligned with the Early Treatment of Diabetic Retinopathy Study (ETDRS) grid (shown in *insert* with dimension of 100/300/600  $\mu\text{m}$  for mouse retina). (F) Averaged changes in OP length after 15 minutes and 2 hours of LA (left), or after 15 minutes and 2 hours of DA (right). \* $P < 0.05$ , \*\*\* $P < 0.01$ .

could be detected in the OCT image, with an average extension of OSEL length of  $2.1 \pm 0.3 \mu\text{m}$  ( $n = 9$ ,  $P < 0.001$ ) under light exposure and an average contraction of  $1.4 \pm 0.4 \mu\text{m}$  ( $n = 7$ ,  $P < 0.05$ ) for dark exposure. Larger magnitude OSEL length changes were detected after 2 hours of either LA or DA. An average extension of the OSEL length of  $4.1 \pm 0.9 \mu\text{m}$  ( $n = 6$ ,  $P < 0.01$ ) was observed for 2 hours of light exposures, while a contraction of the OSEL length of  $3.0 \pm 0.5 \mu\text{m}$  ( $n = 8$ ,  $P < 0.01$ ) was observed for 2 hours of dark exposures (Fig. 2F).

### Histologic Changes in the Retina Under LA and DA Conditions

As OCT images provide only optical reflectivity measurements of the changes in the retinal thickness profile with adaptation, we also performed histologic measurements of the LA/DA thickness of the retinal layers. Fluorescently-tagged probes were used to label histologic landmarks and cell boundaries in vibratome-cut retinal sections. Retina regions approximately

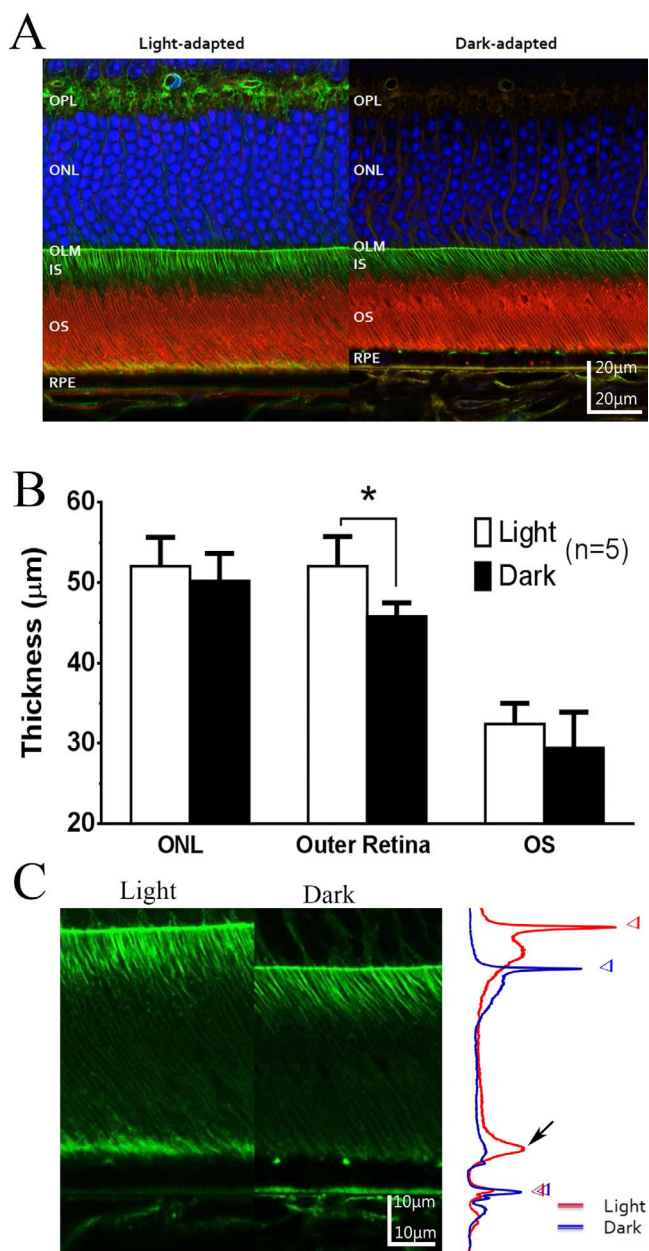


**FIGURE 3.** Histology changes in the mouse retinal structure observed under LA and DA conditions. (A) Examples of confocal images of the outer retina stained with DAPI (for nuclei, blue), phalloidin (for actin filaments, green), and WGA (for rod photoreceptor outer segments, red) from an LA (left) and DA (right) mouse eye. Images are aligned at OLM. (B) Averaged thickness of the retinal layers measured for each color channel from images obtained from LA ( $n = 5$ ) and DA ( $n = 5$ ) eyes.  $*P < 0.05$ . (C) Example of the phalloidin staining pattern for F-actin from the OLM to the choroid in LA and DA retinas. Images are aligned at the RPE layer. Comparison of phalloidin intensity profiles (right) for retinas from LA (red line) and DA (blue line) conditions showed LA caused actin to be localized to RPE apical processes. Open triangles point to the peaks used to measure OLM-BM length. Black arrow points to a peak of green intensity only observed on images of LA retina.

400  $\mu\text{m}$  away from optic nerve head were selected, and measurements were made at two locations for each eye and averaged. Figure 3A shows confocal images of the outer retina stained with DAPI (for nuclei, blue), phalloidin (for actin filaments, green), and WGA (for rod photoreceptor OS, red)

from a LA mouse eye (left) and a DA mouse eye (right). Images were aligned at the level of OLM. While the thickness of the outer nuclear layer (ONL) is similar in both eyes, there is a large difference in the “outer retina” (between OLM and BM) thickness in LA eyes compared to their DA counterparts. We used intensity profiles of each confocal microscope color channel to measure quantitatively the thickness of the retinal layers. These results are summarized in the bar graph in Figure 3B. Staining with DAPI (blue channel) was used to measure the thickness of the ONL. No statistical difference was detected in the mean thickness of ONL under LA and DA conditions. Phalloidin staining for F-actin (green channel) was used to measure the thickness of the outer retina (between OLM and BM). An example of an intensity profile for green channel is shown in Figure 3C, right. Intensity peaks can be observed clearly at the OLM and BM (marked by triangles). On average, the histologically measured outer retina length was  $52.1 \pm 3.7 \mu\text{m}$  ( $n = 5$ ) for LA eyes and  $45.8 \pm 1.7 \mu\text{m}$  ( $n = 5$ ) for DA eyes. This difference was statistically significant ( $P < 0.01$ ), and comparable in magnitude with our changes observed in OCT images ( $56.9 \pm 1.7$  and  $50.1 \pm 1.7 \mu\text{m}$  for LA/DA conditions, respectively Figure 2B).<sup>14</sup> The WGA lectin stain (red channel) was used for measuring the length of the rod photoreceptor OS. The OS length in the DA mouse retina were a little shorter than in the LA retina, but the difference was not statistically significant ( $P > 0.2$ ,  $n = 5$ ).

In addition to the differences observed in the length in the outer mouse retina, there also were distinct changes in the outer retinal phalloidin staining pattern in the LA versus DA conditions. Figure 3C shows an example of the phalloidin staining in the distal region of the mouse retina under LA and DA conditions, and images are aligned at BM. The phalloidin staining on the apical side of the RPE extends as a broad band surrounding the tips of the photoreceptor OS in the LA retina, while the phalloidin-positive band was absent in the DA retina. This difference also could be observed in the phalloidin stain intensity profiles, as shown in the right of Figure 3C. A high intensity peak is observed (black arrow) next to the RPE apical region in the LA retina, which is absent in the DA retina. To quantitate this difference, we measured green peak intensities in regions next to the apical RPE (5  $\mu\text{m}$  from RPE border) and those in the center of photoreceptor OS. The ratio of intensity at these two regions from LA eyes was  $6.1 \pm 3.3$  ( $n = 5$ ), while the ratio declined under DA to  $1.8 \pm 0.8$  ( $n = 5$ ,  $P < 0.05$ ). On the other hand, intensity of phalloidin staining at the base side of RPE was much stronger in DA retinas than those under LA conditions. The peak intensity ratio of apical-peak to basal-peak was  $2.4 \pm 1.8$  ( $n = 5$ ) for LA retinas and  $0.4 \pm 1.6$  ( $n = 5$ ,  $P < 0.05$ ) for DA retinas. In other words, LA appears to induce a redistribution of actin filaments from the basal side to apical villi in RPE cells.

## DISCUSSION

Using ultra high resolution OCT imaging, we observed light-induced dimensional changes in the mouse retinal layers which were principally located in the outer retina. Comparing the normal LA (~5 hours) retina to the same eye after overnight DA, the “outer-retina” (i.e., OLM-to-BM) length increased approximately 6  $\mu\text{m}$ . This was the maximum change we observed under normal physiological conditions. No additional elongation of “outer-retina” length was observed when mice were kept in prolonged LA for 24 hours compared to the same eye under approximately 5 hours of room light (data not shown). Similarly, prolonged DA did not induce further retraction of “outer-retina” length when compared to the same eye after overnight DA. In fact, we observed a slight

( $\sim 2.5 \mu\text{m}$ ) elongation of “outer-retina” length for the eyes after 8 days in dark, which is consistent with photostasis mechanisms reported by others for rodent eyes.<sup>15–17</sup>

The effects of light or dark exposure on changes in the “outer-retina” length observed in OCT images were slow. With 15 minutes of either light or dark exposure, small but significant changes in OSEL length could be detected reliably. Reliable detection of these changes depends on comparing OCT images from the same eye, and the axial resolution of the OCT imager system. With 2 hours of exposure to light or dark, OSEL length alterations averaged  $+4.1$  and  $-3.0 \mu\text{m}$ , respectively (Fig. 2F). However, the detailed kinetics of these light-evoked dimensional changes needs further investigation with OCT.

Optical coherence tomography produces an image through relative light reflection/scattering in the tissue along the optical path (retinal depth). Therefore, alterations in either the physical length of the retina or the optical index of refraction of the retinal media could change the depth profile of the retinal layers observed in the OCT image. Indeed, it has been reported that components of extracellular matrix around photoreceptor outer segment varies with LA and DA,<sup>18,19</sup> although the effects of these extracellular matrix proteins on the refractive index of photoreceptor outer segments is unknown. However, we observed similar LA/DA magnitudes of “outer-retina” length changes in OCT images as physical distance changes on the histologic sections. These results suggest that the physical changes in outer retinal region of the mouse under LA and DA conditions are the major factors mediating the changes observed in the OCT image. On the other hand, while LA/DA changes in the OCT image were localized mainly to the OSEL, which include the hyporeflexive band of LA retina in our measurement, only small and statistically insignificant changes in OS length were observed on histologic sections. As histologic studies of LA/DA changes must be compared from eyes from different animals, there are unavoidable individual variations. In addition, although great care was taken to preserve the retinal tissue at native status with our fixation protocol (i.e., undehydrated), it still is possible that our histologic procedures might introduce some dimensional alterations to the retina.

We observed a number of retinal mechanisms that could mediate LA/DA changes in the distal regions of the mouse retina. It is well-known that the tips of rod photoreceptor outer segment are phagocytized by RPE cells (disk shedding). This disk shedding activity is influenced by the circadian rhythm and duration of light exposure.<sup>20–22</sup> Most of our studies were performed at the same subjective day time for LA and DA. Therefore, the circadian rhythm should have minimal effects on our light-evoked OCT changes. Rod photoreceptor disk shedding is most active in the first 2 hours after light onset in the morning, and less active immediately after light-offset in the evening.<sup>20,23,24</sup> Most of our experiments were conducted in the late morning to early afternoon, a time period with stable disk shedding activity. It has been reported that this stable disk shedding activity could be more active for animals kept in dark than those exposed to modulated light.<sup>25</sup> This is consistent with some small, although statistically insignificant, changes in photoreceptor outer segment length observed on histologic sections (Fig. 3).

Light also is reported to elicit a significant change in the hydration (volume) of the subretinal space in vertebrate eyes, when measured with selective electrodes for membrane impermeable ions.<sup>26–28</sup> Similarly, using NMR techniques, expansion of water diffusion in the subretinal space also has been detected in rodent eyes.<sup>29,30</sup> These results are consistent with our observations on light-evoked OCT responses imaged in the rod-dominant mouse eye. Accumulation of fluid in the subretinal space could explain the appearance of the hyporeflexive band between the RPE and PRT on the OCT image

under LA conditions. This expansion of subretinal space also might account for the “outer-retina” distance changes. As the OLM and apical side of RPE cells are sealed with tight junctions, accumulation of subretinal fluid can only lead to an expansion in a longitudinal direction. Although the mechanism for enhanced phalloidin (actin) staining on the apical side of RPE microvilli in the LA condition is not clear, accumulation of fluid in the subretinal space and alteration in volume (and possibly the tension) in the outer region of the retina could have a role in changing the morphology of the RPE microvilli.

It will be interesting to determine if human retina also exhibits similar dimensional changes in the OCT image with LA. Abramoff et al.<sup>13</sup> compared OCT images obtained with a commercial OCT system (Heidelberg Spectralis; Heidelberg Engineering, Heidelberg, Germany) for normal human subjects and Best macular dystrophy patients during a 40-minute dark-light cycle. Their study was focused on structural changes in the foveal region where Best disease is manifested. A decrease of approximately  $2 \mu\text{m}$  in OSEL length after 10 to 20 minutes' light adaptation was reported in normal subjects.<sup>13</sup> These observations on the human fovea are opposite to what we observed in the mouse eye. However, it should be noted that while the photoreceptors OS length shrank, the RPE thickness was increased. In addition, the human fovea thickness OS length reduction observed was transient, and the changes in OSEL length returned to near baseline levels at the end of the 30-minute LA cycle. It should be noted, however, that OCT images differ in the cone-dominant fovea and rod-dominant peripheral retina, particularly in the outer retina. Whereas four retinal bands can be observed in peripheral regions of human eye, PRT and RPE lines often are fused in OCT images of the human fovea. Whether the peripheral region of the human eye, where the retina is rod-dominated like the mouse, also exhibits similar light-evoked OCT thickness changes remain to be determined.

In summary, LA leads to an elongation in outer retinal regions from OLM to RPE cells in the mouse retina, which can be detected in the OCT image and in histologic sections. The response takes minutes to develop and hours to saturate. Although it is likely multiple cellular mechanisms are involved in these light-evoked retinal thickness changes observed in OCT images, one leading candidate is the changes in subretinal fluid regulated by RPE and photoreceptor cell activity. If confirmed, light-evoked OCT response could be used as a noninvasive metric of subretinal fluid transport and RPE cell function in the intact eye.

### Acknowledgments

The authors thank Bruce Berkowitz for insightful discussions.

Supported by the intramural program of the National Eye Institute (Bethesda, MD, USA). The mention of commercial products, their sources, or their use in connection with material reported herein is not to be construed as either an actual or implied endorsement of such products by the Department of Health and Human Services.

Disclosure: **Y. Li**, None; **R.N. Fariss**, None; **J.W. Qian**, None; **E.D. Cohen**, None; **H. Qian**, None

### References

- Adhi M, Duker JS. Optical coherence tomography—current and future applications. *Curr Opin Ophthalmol*. 2013;24:213–221.
- Costa RA, Skaf M, Melo LA Jr, et al. Retinal assessment using optical coherence tomography. *Prog Retin Eye Res*. 2006;25:325–353.
- Zhang QX, Lu RW, Messinger JD, Curcio CA, Guarcello V, Yao XC. In vivo optical coherence tomography of light-driven

- melanosome translocation in retinal pigment epithelium. *Sci Rep*. 2013;3:2644.
4. Bizheva K, Pflug R, Hermann B, et al. Optophysiology: depth-resolved probing of retinal physiology with functional ultrahigh-resolution optical coherence tomography. *Proc Natl Acad Sci U S A*. 2006;103:5066-5071.
  5. Majdi JA, Qian H, Li Y, et al. The use of time-lapse optical coherence tomography to image the effects of microapplied toxins on the retina. *Invest Ophthalmol Vis Sci*. 2015;56:587-597.
  6. Fujimoto JG. Optical coherence tomography for ultrahigh resolution in vivo imaging. *Nat Biotechnol*. 2003;21:1361-1367.
  7. Spaide RF, Curcio CA. Anatomical correlates to the bands seen in the outer retina by optical coherence tomography: literature review and model. *Retina*. 2011;31:1609-1619.
  8. Staurengi G, Sadda S, Chakravarthy U, Spaide RF. International Nomenclature for Optical Coherence Tomography P. Proposed lexicon for anatomic landmarks in normal posterior segment spectral-domain optical coherence tomography: the IN<sup>3</sup>OCT consensus. *Ophthalmology*. 2014;121:1572-1578.
  9. Saxena S, Srivastav K, Cheung CM, Ng JY, Lai TY. Photoreceptor inner segment ellipsoid band integrity on spectral domain optical coherence tomography. *Clin Ophthalmol*. 2014;8:2507-2522.
  10. Jonnal RS, Kocaoglu OP, Zawadzki RJ, Lee SH, Werner JS, Miller DT. The cellular origins of the outer retinal bands in optical coherence tomography images. *Invest Ophthalmol Vis Sci*. 2014;55:7904-7918.
  11. Mitamura Y, Mitamura-Aizawa S, Katome T, et al. Photoreceptor impairment and restoration on optical coherence tomographic image. *J Ophthalmol*. 2013;2013:518170.
  12. Hale IL, Matsumoto B. Resolution of subcellular detail in thick tissue sections: immunohistochemical preparation and fluorescence confocal microscopy. *Methods Cell Biol*. 2002;70:301-335.
  13. Abramoff MD, Mullins RF, Lee K, et al. Human photoreceptor outer segments shorten during light adaptation. *Invest Ophthalmol Vis Sci*. 2013;54:3721-3728.
  14. Berger A, Cavallero S, Dominguez E, et al. Spectral-domain optical coherence tomography of the rodent eye: highlighting layers of the outer retina using signal averaging and comparison with histology. *PLoS One*. 2014;9:e96494.
  15. Cunea A, Begum R, Reinisch D, Jeffery G. Questioning photostasis. *Vis Neurosci*. 2013;30:169-174.
  16. Penn JS, Williams TP. Photostasis: regulation of daily photon-catch by rat retinas in response to various cyclic illuminances. *Exp Eye Res*. 1986;43:915-928.
  17. Daly GH, DiLeonardo JM, Balkema NR, Balkema GW. The relationship between ambient lighting conditions, absolute dark-adapted thresholds, and rhodopsin in black and hypopigmented mice. *Vis Neurosci*. 2004;21:925-934.
  18. Uehara F, Matthes MT, Yasumura D, LaVail MM. Light-evoked changes in the interphotoreceptor matrix. *Science*. 1990;248:1633-1636.
  19. Uehara F, Yasumura D, LaVail MM. Rod- and cone-associated interphotoreceptor matrix in the rat retina. Differences in light-evoked distributional changes. *Invest Ophthalmol Vis Sci*. 1991;32:285-292.
  20. LaVail MM. Rod outer segment disk shedding in rat retina: relationship to cyclic lighting. *Science*. 1976;194:1071-1074.
  21. Bobu C, Hicks D. Regulation of retinal photoreceptor phagocytosis in a diurnal mammal by circadian clocks and ambient lighting. *Invest Ophthalmol Vis Sci*. 2009;50:3495-3502.
  22. Goldman AI. The sensitivity of rat rod outer segment disc shedding to light. *Invest Ophthalmol Vis Sci*. 1982;22:695-700.
  23. Goldman AI, Teirstein PS, O'Brien PJ. The role of ambient lighting in circadian disc shedding in the rod outer segment of the rat retina. *Invest Ophthalmol Vis Sci*. 1980;19:1257-1267.
  24. LaVail MM. Outer segment disc shedding and phagocytosis in the outer retina. *Trans Ophthalmol Soc U K*. 1983;103:397-404.
  25. Baker BN, Moriya M, Williams TP. Alteration of disk-shedding patterns by light-onset of higher than normal intensity. *Exp Eye Res*. 1986;42:535-546.
  26. Huang B, Karwoski CJ. Light-evoked expansion of subretinal space volume in the retina of the frog. *J Neurosci*. 1992;12:4243-4252.
  27. Li JD, Gallemore RP, Dmitriev A, Steinberg RH. Light-dependent hydration of the space surrounding photoreceptors in chick retina. *Invest Ophthalmol Vis Sci*. 1994;35:2700-2711.
  28. Li JD, Govardovskii VI, Steinberg RH. Light-dependent hydration of the space surrounding photoreceptors in the cat retina. *Vis Neurosci*. 1994;11:743-752.
  29. Berkowitz BA, Grady EM, Khetarpal N, Patel A, Roberts R. Oxidative stress and light-evoked responses of the posterior segment in a mouse model of diabetic retinopathy. *Invest Ophthalmol Vis Sci*. 2015;56:606-615.
  30. Bissig D, Berkowitz BA. Light-dependent changes in outer retinal water diffusion in rats in vivo. *Mol Vis*. 2012;18:2561-2577.